

Frequency mixing in a ferrimagnetic sphere resonator

Cijy Mathai,¹ Sergei Masis,¹ Oleg Shtempluck,¹ Shay Hacoheh-Gourgy,² and Eyal Buks¹

¹Andrew and Erna Viterbi Department of Electrical Engineering, Technion, Haifa 32000 Israel

²Physics Department, Technion, Haifa 32000 Israel

(Dated: May 21, 2020)

Frequency mixing in ferrimagnetic resonators based on yttrium and calcium vanadium iron garnets (YIG and CVBIG) is employed for studying their nonlinear interactions. The ferrimagnetic Kittel mode is driven by applying a pump tone at a frequency close to resonance. We explore two nonlinear frequency mixing configurations. In the first one, mixing between a transverse pump tone and an added longitudinal weak signal is explored, and the experimental results are compared with the predictions of the Landau-Zener-Stuckelberg model. In the second one, intermodulation measurements are employed by mixing pump and signal tones both in the transverse direction for studying a bifurcation between a stable spiral and a stable node attractors. Our results are applicable for developing sensitive signal receivers with high gain for both the radio frequency and the microwave bands.

I. INTRODUCTION

The physics of magnons in ferromagnetic resonators [1–3] has been extensively studied in the backdrop of Bose-Einstein condensation [4], optomagnonics [5–7], and spintronics [8]. Owing to the high magnon life time of the order of a few microseconds, such ferromagnetic insulators have become the natural choice of microwave (MW) resonators in synthesizers [9], narrow band filters [10], and parametric amplifiers [11]. Exploring the nonlinearity associated with such systems is gaining attention. A variety of magnon *nonlinear* dynamical effects have been studied in the context of auto-oscillations [12], optical cooling [13], frequency mixing [14, 15] and bistability [16–20]. Applications of nonlinearity for quantum data processing have been explored in [21, 22]. Nonlinear interactions between the electromagnetic (EM) MW field coherent photons and these resonators can be significantly enhanced with relatively low power around the resonance frequency of the oscillator. Studying such nonlinear interactions is important due to the realization of hybrid quantum systems for quantum memory and optical transducer related applications [23–28].

Here we study the nonlinear frequency mixing process in these ferromagnetic resonators based on two configurations. In the first configuration we study frequency mixing of transverse and longitudinal driving tones that are simultaneously applied to the magnon resonator. The signal tone is in the radio frequency (RF) band, and it is applied in the longitudinal direction, parallel to the external static magnetic field. This process can be employed for frequency conversion between the RF and the MW bands. Here we find that the measured response can be well described using the Landau-Zener-Stuckelberg model [29, 30]. In the second configuration, Kerr nonlinearity that is induced by magnetic anisotropy is studied by intermodulation measurements. This is done by simultaneously applying in the transverse direction an intense pump and a weak signal tones both having frequencies close to resonance. The observed intermodulation frequency conversion reveals a bifurcation between a

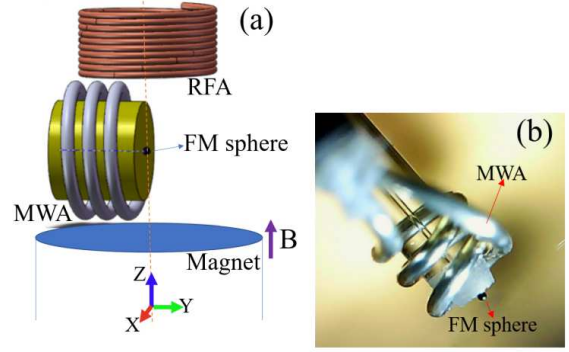


FIG. 1: (a) A schematic of the experimental setup used for studying the ferrimagnetic (FM) sphere. Longitudinal and transverse driving are applied using a radio frequency antenna (RFA) and a microwave antenna (MWA), respectively. (b) Real image of the DUT.

stable spiral and a stable node [31]. These nonlinear effects may find applications in signal sensing, parametric amplification and other related applications.

The spherical resonators under test are made of yttrium iron garnet (YIG) and calcium vanadium bismuth iron garnet (CVBIG) with a radius of $R_s = 125 \mu\text{m}$. They host magnonic excitations with relatively low damping and large spin densities. These spheres are anisotropic ferrimagnetic crystals with strong Faraday rotation angles and high refractive index as compared to other iron garnets. A schematic image of our device under test (DUT) is shown in Fig. 1. The ferrimagnetic sphere is held by vacuum through a ferrule. A fixed magnet is employed for fully magnetizing the sphere. A loop antenna (coil) is used to apply a transverse (longitudinal) driving in the MW (RF) band. All measurements are performed at room temperature.

II. LANDAU-ZENER-STUCKELBERG INTERFEROMETRY

Landau-Zener-Stuckelberg interferometry is based on a mixing process between transverse and longitudinal driving frequencies that are simultaneously applied to a resonator [29, 30]. The polarization vector \mathbf{P} evolves in time t according to the Bloch-Landau-Lifshitz equation $d\mathbf{P}/dt = \mathbf{P} \times \boldsymbol{\Omega} + \boldsymbol{\Gamma}$, where $\boldsymbol{\Omega} = \gamma_e \mathbf{B}$ is the rotation vector, with \mathbf{B} being the externally applied magnetic induction and $\gamma_e = 28 \text{ GHz T}^{-1}$ being the gyromagnetic ratio, and the vector $\boldsymbol{\Gamma} = -\Gamma_2 P_x \hat{\mathbf{x}} - \Gamma_2 P_y \hat{\mathbf{y}} - \Gamma_1 (P_z - P_{z,s}) \hat{\mathbf{z}}$ represents the contribution of damping, with $\Gamma_1 = 1/T_1$ and $\Gamma_2 = 1/T_2$ being the longitudinal and transverse relaxation rates, respectively, and $P_{z,s}$ being the steady state polarization. Consider the case where $\boldsymbol{\Omega}(t) = \omega_1 (\cos(\omega t) \hat{\mathbf{x}} + \sin(\omega t) \hat{\mathbf{y}}) + \omega_0 \hat{\mathbf{z}}$. Here ω_1 and ω are both real constants, and ω_0 oscillates in time according to $\omega_0 = \omega_c + \omega_b \sin(\omega_m t)$, where ω_c , ω_b and ω_m are all real constants. Nonlinearity of the Bloch-Landau-Lifshitz equation gives rise to frequency mixing between the transverse driving at angular frequency ω and the longitudinal driving at angular frequency ω_m . The resonance condition of the l 'th order frequency mixing process reads $\omega + l\omega_m = \omega_c$, where l is an integer. The complex amplitude P_+ (in a rotating frame) of the corresponding l 'th side band is given by (see appendix D of Ref. [32])

$$P_+ = \frac{\frac{i\omega_1 \zeta}{\Gamma_2^2} \left(1 + \frac{i\omega_d}{\Gamma_2}\right) P_{z,s}}{\left(1 + \frac{\omega_d^2}{\Gamma_2^2}\right) \frac{\Gamma_1}{\Gamma_2} + \left(\frac{\omega_1 \zeta}{\Gamma_2}\right)^2}, \quad (1)$$

where $\zeta = J_l(\omega_b/\omega_m)$, J_l is the l 'th Bessel function of the first kind, and the detuning angular frequency ω_d is given by $\omega_d = \omega + l\omega_m - \omega_c$.

The schematic of the experimental setup employed to explore this frequency mixing process is shown in Fig. 2 (a). The device under test (DUT₁) comprises of the ferrimagnetic resonator coupled to both the MW loop antenna and the RF coil. The Kittel mode frequency is tuned by the static magnetic field to the value 2.305 GHz. The sphere is simultaneously driven by a pump with a power of 0 dBm that is applied to the MW loop antenna and an RF signal with a frequency of 0.5 MHz that is applied to the RF coil. Spectrum analyzer measurements of the signal reflected from the MW loop antenna are shown in Fig. 2 (b) as a function of the spectrum analyzer angular frequency ω_{SA} and the driving MW angular frequency ω_{MW} that is injected into the loop antenna. The theoretical prediction that is derived using Eq. (1) is presented by Fig. 2 (c). The values of parameters that are used for the calculation are listed in the caption of Fig. 2. The comparison between the measured [see Fig. 2 (b)] and calculated [see Fig. 2 (c)] response yields a good agreement.

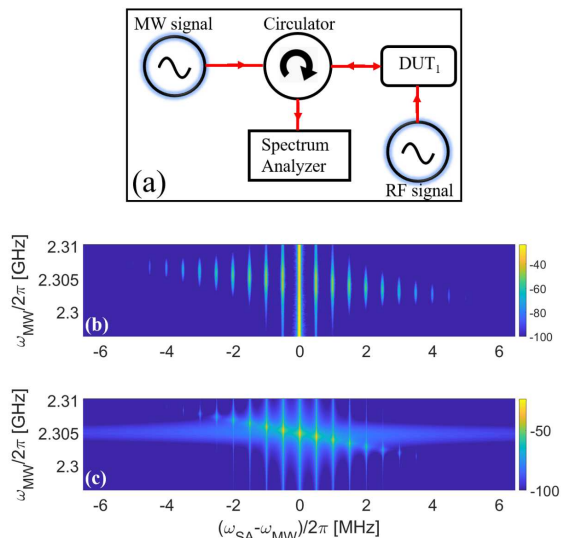


FIG. 2: Landau-Zener-Stuckelberg interferometry. Experimental (b) and theoretical (c) spectral response obtained by the frequency mixing of transverse and longitudinal driving signals applied simultaneously to the magnon resonator. The theoretical color-coded plot (c) is derived using Eq. (1), using the following parameters' values $\omega_m/(2\pi) = 0.5 \text{ MHz}$, $\omega_1/(2\pi) = 0.5 \text{ MHz}$, $\omega_b/(2\pi) = 0.5 \text{ MHz}$, $\Gamma_1/(2\pi) = 1.0 \text{ MHz}$ and $\Gamma_2/(2\pi) = 2.0 \text{ MHz}$.

III. ANISOTROPY-INDUCED KERR NONLINEARITY

The experimental setup used for intermodulation measurements is shown in Fig. 3 (a). Here the device under test (DUT₂) is the same as that shown in Fig. 1, where the RF antenna (RFA) is removed from the setup. The nonlinearity gives rise to bistability, which in turn yields a hysteretic resonance curve, which is obtained via the forward and backward sweeping directions [see Fig. 3 (b)]. The measured response becomes bistable when the input pump power P_p is of the order of mW. The subsequent idler tones generated due to the nonlinear frequency mixing of pump and signal tones in the ferrimagnetic resonator are shown in Fig. 3(c).

The technique of Bosonization can be applied to model the nonlinearity in ferrimagnetic sphere resonators [33]. In this approach, the Hamiltonian \mathcal{H}_M is expressed in the form $\hbar^{-1}\mathcal{H}_M = \omega_c N_M + K_M N_M^2 + Q_M N_M^4 + \dots$, where $\omega_c = \mu_0 \gamma_e H$ is the angular frequency of the Kittel mode [7, 34], $\mu_0 = 4\pi \times 10^{-7} \text{ N A}^{-2}$ is the permeability of free space, H is the externally applied uniform magnetic field (which is assumed to be parallel to the $\hat{\mathbf{z}}$ axis), N_M is a number operator, K_M is the so-called Kerr frequency, and Q_M is the coefficient of quartic nonlinearity. When nonlinearity is taken into account to lowest nonvanishing order only, i.e. when the quartic and all higher order terms are disregarded, the response can be described using the Duffing-Kerr model. This model predicts that the response of the system to an externally applied monochro-

matic driving can become bistable.

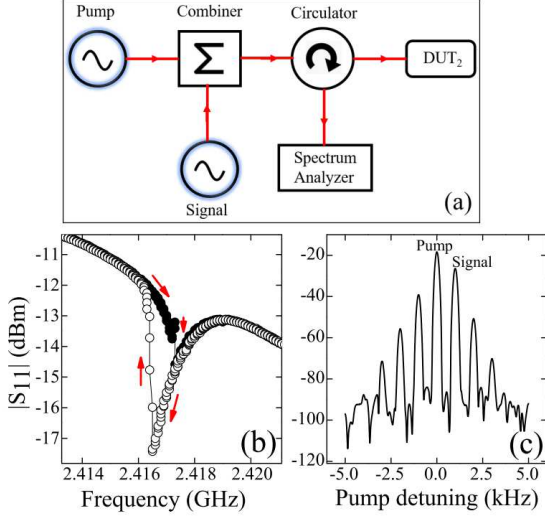


FIG. 3: Intermodulation. (a) An intense pump and a relatively weak signal are simultaneously injected into the MW loop antenna, and the reflected signal is measured using a spectrum analyzer. (b) Experimentally obtained hysteric resonance curve (with no signal) showing bistability corresponding to the forward and backward microwave frequency sweep directions. (c) Spectrum analyzer measurement of the reflected signal intensity as a function of the detuning frequency with respect to the pump frequency. The idler peaks are generated as a result of the nonlinear pump-signal mixing.

In general, the number of magnons $\langle N_M \rangle$ in a resonantly driven sphere having total linear damping rate γ_c with pump power P_p is given for the case of critical coupling by $\langle N_M \rangle \simeq P_p / (\hbar\omega_c\gamma_c)$. On the other hand, the expected number of magnons $\langle N_M \rangle$ at the onset of Duffing-Kerr bistability is $\simeq \gamma_c / |K_M|$ [see Eq. (42) of Ref. [35] and note that, for simplicity, cubic nonlinear damping is disregarded]. Thus, from the measured values of the linear damping rate $\gamma_c / (2\pi) \simeq 1$ MHz and $P_p \simeq 1$ mW, at the bistability onset point one obtains $K_M / (2\pi) \simeq -2 \times 10^{-9}$ Hz (the minus signs indicates that the Kerr nonlinearity gives rise to softening). Note, however, that the above estimate, which is based on the Duffing-Kerr model, is valid provided that the quartic and all higher order terms can be disregarded near (and below) the bistability onset. For the quartic term this condition can be expressed as $|Q_M| \ll |K_M|^3 / \gamma_c^2$.

The values of K_M and Q_M are estimated below for the case where nonlinearity originates from magnetic anisotropy. The Stoner-Wohlfarth energy E_M is expressed as a function of the magnetization vector $\mathbf{M} = M\hat{\mathbf{u}}_M$, and the first-order K_{c1} and second-order K_{c2} anisotropy constants as [36]

$$\frac{E_M}{V_s} = -\mu_0 \mathbf{M} \cdot \mathbf{H} + K_{c1} \sin^2 \phi + K_{c2} \sin^4 \phi, \quad (2)$$

where $V_s = 4\pi R_s^3/3$ is the volume of the sphere having radius R_s , and ϕ is the angle between $\hat{\mathbf{u}}_M$ and the

unit vector $\hat{\mathbf{u}}_A$ parallel to the easy axis. It is assumed that the sphere is fully magnetized, i.e. $|\mathbf{M}| \simeq M_s$, where M_s is the saturation magnetization. In terms of the dimensionless angular momentum vector $\boldsymbol{\Sigma} = -2M_s V_s / (\hbar\gamma_e) \equiv (\Sigma_x, \Sigma_y, \Sigma_z)$ Eq. (2) is rewritten as $E_M - \hbar\omega_{K1} (1 + K_{c2}/K_{c1}) = \mathcal{H}_M$, where

$$\begin{aligned} \hbar^{-1} \mathcal{H}_M = & \frac{\omega_c \Sigma_z}{2} + \left(1 + \frac{2K_{c2}}{K_{c1}}\right) \frac{K_M (\boldsymbol{\Sigma} \cdot \hat{\mathbf{u}}_A)^2}{4} \\ & + \frac{K_{c2}}{K_{c1}} \frac{K_M^2 (\boldsymbol{\Sigma} \cdot \hat{\mathbf{u}}_A)^4}{16\omega_{K1}}, \end{aligned} \quad (3)$$

$\omega_{K1} = \hbar^{-1} V_s K_{c1}$ and $K_M = \hbar\gamma_e^2 K_{c1} / (V_s M_s^2)$ is the Kerr frequency [17].

In the Holstein-Primakoff transformation [37], the operators $\Sigma_{\pm} = \Sigma_x \pm i\Sigma_y$ and Σ_z are expressed as $\Sigma_+ = B^\dagger (N_s - N'_M)^{1/2}$, $\Sigma_- = (N_s - N'_M)^{1/2} B$ and $\Sigma_z = -N_s + 2N'_M$, where N_s is the total number of spins, and where $N'_M = B^\dagger B$ is a number operator. If the operator B satisfies the Bosonic commutation relation $[B, B^\dagger] = 1$ then the following holds $[\Sigma_z, \Sigma_+] = 2\Sigma_+$, $[\Sigma_z, \Sigma_-] = -2\Sigma_-$ and $[\Sigma_+, \Sigma_-] = \Sigma_z$. The approximation $(N_s - N'_M)^{1/2} \simeq N_s^{1/2}$ leads to $\boldsymbol{\Sigma} \cdot \hat{\mathbf{u}}_A = N_s^{1/2} (B^\dagger u_{A+} + B u_{A-}) + 2N'_M u_{Az}$, where $u_{A\pm} = [(\hat{\mathbf{u}}_A \cdot \hat{\mathbf{x}}) \mp i(\hat{\mathbf{u}}_A \cdot \hat{\mathbf{y}})]/2$, $u_{Az} = \hat{\mathbf{u}}_A \cdot \hat{\mathbf{z}}$, and the magnon number operator N_M is defined by $N_M = N'_M - N_s/2$. This approximation is valid near the bistability onset provided that $\gamma_c / (|K_M| N_s) \ll 1$. For YIG, the spin density is $\rho_s = 4.2 \times 10^{21} \text{ cm}^{-3}$, thus for a sphere of radius $R_s = 125 \mu\text{m}$ the number of spins is $N_s = V_s \rho_s = 3.4 \times 10^{16}$, hence for the current experiment $\gamma_c / (|K_M| N_s) \simeq 10^{-1}$. This estimate suggests that inaccuracy originating from this approximation may be significant for the current experiment near and above the bistability threshold.

Second-order anisotropy gives rise to a quartic nonlinear term in the Hamiltonian (3) with a coefficient $Q_M \simeq (K_{c2}/K_{c1}) (K_M^2 / \omega_{K1})$ (the exact value depends on the angle ϕ between the magnetization vector and the easy axis). Near or below the bistability onset the quartic term can be safely disregarded provided that $(K_{c2}/K_{c1}) (\gamma_c^2 / (\omega_{K1} |K_M|)) \ll 1$. When this condition is satisfied the Hamiltonian (3) for the case where $\hat{\mathbf{u}}_A$ is parallel to $\hat{\mathbf{z}}$ (i.e. $u_{Az} = 1$ and $u_{A+} = u_{A-} = 0$) approximately becomes

$$\hbar^{-1} \mathcal{H}_M = \omega_c N_M + K_M N_M^2. \quad (4)$$

The term proportional to K_M represents the anisotropy-induced Kerr nonlinearity.

For YIG $M_s = 140 \text{ kA/m}$, $K_{c1} = -610 \text{ J/m}^3$ at 297 K (room temperature), hence for a sphere of radius $R_s = 125 \mu\text{m}$ the expected value of the Kerr coefficient is given by $K_M / (2\pi) = -2.0 \times 10^{-9} \text{ Hz}$. This value well agrees with the above estimation of $K_M / (2\pi)$ based on the measured input power at the bistability onset. For YIG $K_{c2}/K_{c1} = 4.8 \times 10^{-2}$ ($K_{c2}/K_{c1} = 4.3 \times 10^{-2}$) at a temperature of $T = 4.2 \text{ K}$ ($T = 294 \text{ K}$) [7]. Based on these

values one finds that for the sphere resonators used in the current experiment (K_{c2}/K_{c1}) ($\gamma_c^2/(\omega_{K1}|K_M|)$) $\simeq 10^{-6}$, hence the second-order anisotropy term (proportional to K_{c2}) in Eq. (3) can be safely disregarded in the vicinity of the bistability onset.

IV. STABLE SPIRAL AND STABLE NODE

To explore the regime of weak nonlinear response, consider a resonator being driven by a monochromatic pump tone having amplitude b_c and angular frequency ω_p . The time evolution in a frame rotating at the pump driving frequency is assumed to have the form

$$\frac{dC_c}{dt} + \Theta_c = F_c, \quad (5)$$

where the operator C_c is related to the resonator's annihilation operator A_c by $C_c = A_c e^{i\omega_p t}$, the term $\Theta_c = \Theta_c(C_c, C_c^\dagger)$, which is expressed as a function of both C_c and C_c^\dagger , is assumed to be time independent, and F_c is a noise term having a vanishing expectation value. The complex number B_c represents a fixed point, for which $\Theta_c(B_c, B_c^*) = 0$. By expressing the solution as $C_c = B_c + c_c$ and considering the operator c_c as small, one obtains a linearized equation of motion from Eq. (5) given by

$$\frac{dc_c}{dt} + W_1 c_c + W_2 c_c^\dagger = F_c, \quad (6)$$

where $W_1 = \partial\Theta_c/\partial C_c$ and $W_2 = \partial\Theta_c/\partial C_c^\dagger$ (both derivatives are evaluated at the fixed point $C_c = B_c$).

The stability properties of the fixed point depend on the eigenvalues λ_{c1} and λ_{c2} of the 2×2 matrix W , whose elements are given by $W_{11} = W_{22}^* = W_1$ and $W_{12} = W_{21}^* = W_2$ [see Eq. (6)]. In terms of the trace $T_W = W_1 + W_1^*$ and the determinant $D_W = |W_1|^2 - |W_2|^2$ of the matrix W , the eigenvalues are given by $\lambda_{c1} = T_W/2 + v_W$ and $\lambda_{c2} = T_W/2 - v_W$, where the coefficient v_W is given by $v_W = \sqrt{(T_W/2)^2 - D_W}$. Note that in the linear regime, i.e. when $W_2 = 0$, the eigenvalues become $\lambda_{c1} = W_1$ and $\lambda_{c2} = W_1^*$. For the general case, when both λ_{c1} and λ_{c2} have a positive real part, the fixed point is locally stable. Two types of stable fixed points can be identified. For the so-called stable spiral, the coefficient v_W is pure imaginary [i.e. $(T_W/2)^2 - D_W < 0$], and consequently $\lambda_{c2} = \lambda_{c1}^*$, whereas both λ_{c1} and λ_{c2} are pure real for the so-called stable node, for which v_W is pure real. A bifurcation between a stable spiral and a stable node occurs when v_W vanishes.

Further insight can be gained by geometrically analyzing the dynamics near an attractor. To that end the operators c_c and F_c are treated as complex numbers. The equation of motion (6) for the complex variable c_c can be rewritten as $d\bar{\xi}/dt + W'\bar{\xi} = \bar{f}$, where $\bar{\xi} = (\text{Real}(c_c e^{i\phi}), \text{Imag}(c_c e^{i\phi}))^T$ and $\bar{f} =$

$(\text{Real}(F_c e^{i\phi}), \text{Imag}(F_c e^{i\phi}))^T$ are both two-dimensional real vectors, and where the rotation angle ϕ is real. Transformation into the so-called system of principle axes is obtained when the angle ϕ is taken to be given by $e^{2i\phi} = W_1 W_2^*/|W_1 W_2|$. For this case the 2×2 real matrix W' becomes

$$W' = \begin{pmatrix} \cos\theta_1 & -\sin\theta_1 \\ \sin\theta_1 & \cos\theta_1 \end{pmatrix} \begin{pmatrix} W_+ & 0 \\ 0 & W_- \end{pmatrix}, \quad (7)$$

where $\theta_1 = \arg(W_1)$ and where $W_\pm = |W_1| \pm |W_2|$. Thus, multiplication by the matrix W' can be interpreted for this case as a squeezing with coefficients W_\pm followed by a rotation by the angle θ_1 .

The flow near an attractor is governed by the eigenvectors of the 2×2 real matrix W' . For the case where v_W is pure real the angle α_W between these eigenvectors is found to be given by $\sin\alpha_W = v_W/|W_2|$. Thus at the bifurcation between a stable spiral and a stable node, i.e. when $v_W = 0$, the two eigenvectors of W' become parallel to one another. In the opposite limit, when $v_W = |W_2|$, i.e. when W_1 becomes real, and consequently the matrix W becomes Hermitian, the two eigenvectors become orthogonal to one another (i.e. $\alpha_W = \pi/2$).

The bifurcation between a stable spiral and a stable node can be observed by measuring the intermodulation conversion gain G_I of the resonator. This is done by injecting another input tone (in addition to the pump tone), which is commonly referred to as the signal, at angular frequency $\omega_p + \omega$. The intermodulation gain is defined by $G_I(\omega) = |g_I(\omega)|^2$, where $g_I(\omega)$ is the ratio between the output tone at angular frequency $\omega_p - \omega$, which is commonly referred to as the idler, and the input signal at angular frequency $\omega_p + \omega$. In terms of the eigenvalues λ_{c1} and λ_{c2} the gain G_I is given by [35]

$$G_I = \left| \frac{2\gamma_{c1}W_2}{(\lambda_{c1} - i\omega)(\lambda_{c2} - i\omega)} \right|^2, \quad (8)$$

where γ_{c1} is the coupling coefficient (in units of rate) between the feedline that is used to deliver the input and output signals and the resonator. For the case of a stable spiral, i.e. when $\lambda_{c2} = \lambda_{c1}^*$, one has $|(\lambda_{c1} - i\omega)(\lambda_{c2} - i\omega)|^2 = [\lambda'^2 + (\lambda'' - \omega)^2][\lambda'^2 + (\lambda'' + \omega)^2]$, where $\lambda' = \text{Re}\lambda_{c1}$ and $\lambda'' = \text{Im}\lambda_{c1}$ (i.e. $\lambda_{c1} = \lambda' + i\lambda''$), whereas for the case of a stable node, i.e. when both λ_{c1} and λ_{c2} are pure real, one has $|(\lambda_{c1} - i\omega)(\lambda_{c2} - i\omega)|^2 = (\lambda_{c1}^2 + \omega^2)(\lambda_{c2}^2 + \omega^2)$.

For the case of a resonator having Kerr nonlinearity and cubic nonlinear damping Θ_c is given by $\Theta_c = [i\Delta_c + \gamma_c + (iK_c + \gamma_{c3})N_c]C_c + i\sqrt{2\gamma_{c1}}e^{i\phi_{c1}}b_c$, where $\Delta_c = \omega_c - \omega_p$ is the driving detuning, the total rate of linear damping is $\gamma_c = \gamma_{c1} + \gamma_{c2}$, the rate γ_{c1} characterizes the coupling coefficient between the feedline and the resonator, γ_{c2} is the rate of internal linear damping, γ_{c3} is the rate of internal cubic damping, K_c is the Kerr coefficient, $N_c = A_c^\dagger A_c$ is the resonator number operator, and ϕ_{c1} is a phase coefficient charac-

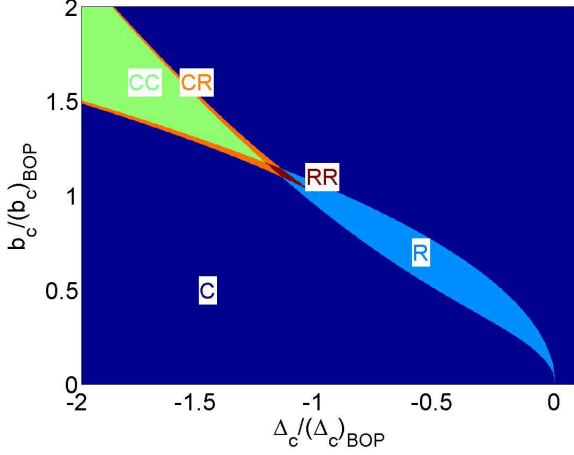


FIG. 4: Stability map of a driven Duffing-Kerr resonator. The BOP is the point $(\Delta_c / (\Delta_c)_{\text{BOP}}, b_c / (b_c)_{\text{BOP}}) = (-1, 1)$. In both 'C' (dark blue) and 'R' (light blue) regions, there is a single locally stable attractor, whereas there are two in the regions 'CC' (light green), 'CR' (orange) and 'RR' (red). The letter 'C' is used to label a stable spiral, whereas the letter 'R' labels a stable node.

terizing the coupling between the feedline and the resonator [35]. The rates W_1 and W_2 are given by $W_1 = i\Delta_c + \gamma_c + 2(iK_c + \gamma_{c3})|B_c|^2$ and $W_2 = (iK_c + \gamma_{c3})B_c^2$. The condition $\Theta_c(B_c, B_c^*) = 0$ can be expressed as a cubic polynomial equation for the number of magnons $E_c = |B_c|^2$ given by $\left[(\Delta_c + K_c E_c)^2 + (\gamma_c + \gamma_{c3} E_c)^2\right] E_c = 2\gamma_{c1} |b_c|^2$. The eigenvalues can be expressed in terms of E_c as $\lambda_{c1,2} = T_W/2 \pm v_W$, where $T_W/2 = \gamma_c + 2\gamma_{c3} E_c$ and $v_W = \sqrt{(\Delta_- - \Delta_c)(\Delta_+ + \Delta_c)}$, where $\Delta_{\pm} = \left(\sqrt{1 + (\gamma_{c3}/K_c)^2} \pm 2\right) K_c E_c$. The stability map of the system is shown in Fig. 4. Both driving detuning Δ_c and driving amplitude b_c are normalized with the corresponding values at the bistability onset point (BOP) $(\Delta_c)_{\text{BOP}}$ and $(b_c)_{\text{BOP}}$ [see Eqs. (46) and (47) of Ref. [35]]. Inside the regions 'C' and 'R' of mono-stability ('CC', 'CR' and 'RR' of bistability) the resonator has one (two) locally stable attractors. A stable spiral (node), for which $\lambda_{c2} = \lambda_{c1}^*$ (both λ_{c1} and λ_{c2} are pure real), is labeled by 'C' ('R').

In the bistable region, the cubic polynomial equation has 3 real solutions for E_c . The corresponding values of the complex amplitude B_c are labeled as C_1 , C_2 and C_3 . In the flow map shown in Fig. 5, which is obtained by numerically integrating the equation of motion (5) for the noiseless case $F_c = 0$, the point C_1 is a stable node, the point C_2 is a saddle point and the point C_3 is a stable spiral. The red and blue lines represent flow toward the stable node attractor at C_1 and the stable spiral attractor at C_3 , respectively. The green line is the separatrix, namely the boundary between the basins of

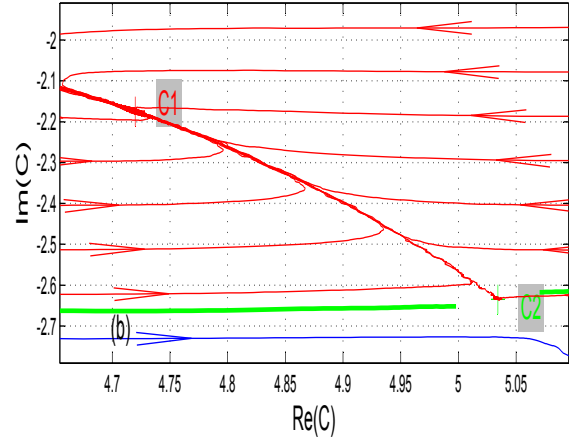
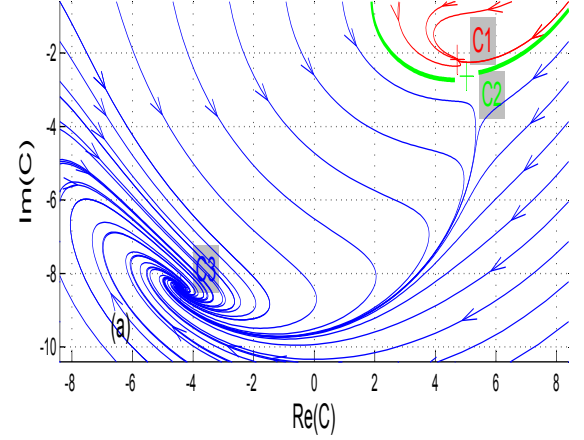


FIG. 5: Flow map of a Duffing oscillator in the region of bistability. The point C_1 is a stable node, the point C_2 is a saddle point, and the point C_3 is a stable spiral. A closer view of the region near C_1 and C_2 is shown in (b).

attraction of the attractors at C_1 and C_3 . A closer view of the region near C_1 and C_2 is shown in Fig. 5(b).

The intermodulation conversion gain G_I induced by the Kerr nonlinearity is measured with the ferrimagnetic resonator DUT₂ [see Fig. 3(a)], and the results are compared with the theoretical prediction given by Eq. (8). In these measurements the pump frequency ω_p is tuned close to the resonance frequency ω_c . The measured gain G_I is shown in the color-coded plots in Fig. 6 (for three different values of the pump frequency ω_p) as a function of the detuning between the signal and pump frequencies $\omega / (2\pi)$ and the pump power P_p .

The overlaid black dotted lines in Fig. 6 indicate the calculated values of the imaginary part of the eigenvalues $\lambda'' = \text{Im} \lambda_{c1}$ and $-\lambda'' = \text{Im} \lambda_{c2}$. The calculation is based on the above-discussed Duffing-Kerr model. At the point

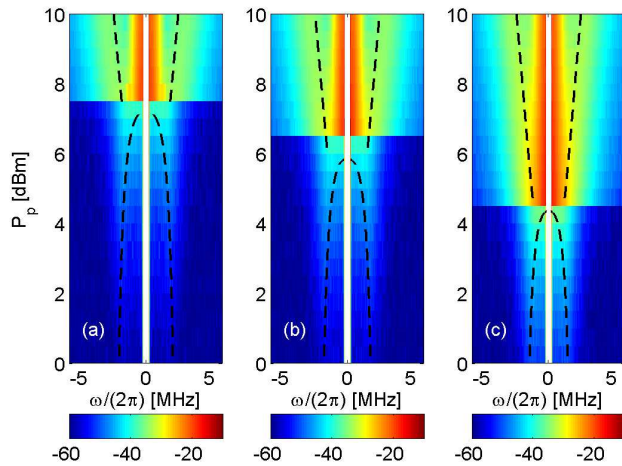


FIG. 6: Intermodulation gain G_I as a function of detuning between the signal and pump frequencies $\omega/(2\pi)$ and pump power P_p (in dBm units). The pump frequency $\omega_p/(2\pi)$ is (a) 3.8674 GHz (b) 3.8704 GHz and (c) 3.8734 GHz. The signal power is -15 dBm. Note that G_I is measured with $\omega > 0$ only, and the plots are generated by mirror reflection of the data around the point $\omega = 0$. Note also that for clarity the region near the pump frequency, i.e. close to $\omega = 0$, has been removed from the plot. The width of this region, in which the intense pump peak is observed, depends on the resolution bandwidth setting of the spectrum analyzer. The black dotted lines indicate the calculated values of the imaginary part of the eigenvalues $\lambda'' = \text{Im } \lambda_{c1}$ and $-\lambda'' = \text{Im } \lambda_{c2}$. The pump amplitude b_c and pump detuning Δ_c used for the calculation of the eigenvalues are determined from the measured value of $P_p = 0.4$ dBm for the pump power and the value of $\Delta_c/(2\pi) = 1.3$ MHz for the pump detuning at the BOP.

where λ'' vanishes, a bifurcation from stable spiral to stable node occurs. As can be seen from comparing panels

(a), (b) and (c) of Fig. 6, the pump power P_p at which this bifurcation occurs depends on the pump frequency ω_p . This bifurcation represents the transition between the regions 'CC' and 'CR' in the stability map shown in Fig. 4. A bifurcation from the bistable to the monostable regions occurs at a higher value of the pump power P_p . This bifurcation gives rise to the sudden change in the measured response shown in Fig. 6. In the stability map shown in Fig. 4, this bifurcation corresponds to the transition between the regions 'CR' and 'C'.

V. CONCLUSION

We present two nonlinear effects that can be used for signal sensing and amplification. The first one is based on the so-called Landau-Zener-Stuckelberg process [29] of frequency mixing between transverse and longitudinal driving tones that are simultaneously applied to the magnon resonator. This process can be employed for frequency conversion between the RF and the MW bands. The second nonlinear effect, which originates from magnetization anisotropy, can be exploited for developing intermodulation receivers in the MW band. Measurements of the intermodulation response near the onset of the Duffing-Kerr bistability reveal a bifurcation between a stable spiral attractor and a stable node attractor. Above this bifurcation, i.e. where the attractor becomes a stable node, the technique of noise squeezing can be employed in order to enhance the signal to noise ratio [35].

VI. ACKNOWLEDGMENTS

We thank Amir Capua for helpful discussions. This work was supported by the Russell Berrie Nanotechnology Institute and the Israel Science Foundation.

-
- [1] Robert M Hill and Robert S Bergman, “Nonlinear response of yig”, *Journal of Applied Physics*, vol. 32, no. 3, pp. S227–S228, 1961.
- [2] RC LeCraw, EG Spencer, and CS Porter, “Ferromagnetic resonance line width in yttrium iron garnet single crystals”, *Physical Review*, vol. 110, no. 6, pp. 1311, 1958.
- [3] Ravinder Kumar, B Samantaray, and Z Hossain, “Ferromagnetic resonance studies of strain tuned bi: Yig films”, *Journal of Physics: Condensed Matter*, vol. 31, no. 43, pp. 435802, 2019.
- [4] SO Demokritov, VE Demidov, O Dzyapko, GA Melkov, AA Serga, B Hillebrands, and AN Slavin, “Bose–einstein condensation of quasi-equilibrium magnons at room temperature under pumping”, *Nature*, vol. 443, no. 7110, pp. 430–433, 2006.
- [5] Xufeng Zhang, Na Zhu, Chang-Ling Zou, and Hong X Tang, “Optomagnonic whispering gallery microresonators”, *Physical review letters*, vol. 117, no. 12, pp. 123605, 2016.
- [6] A Osada, R Hisatomi, A Noguchi, Y Tabuchi, R Yamazaki, K Usami, M Sadgrove, R Yalla, M Nomura, and Y Nakamura, “Cavity optomagnonics with spin-orbit coupled photons”, *Physical review letters*, vol. 116, no. 22, pp. 223601, 2016.
- [7] Daniel D Stancil and Anil Prabhakar, *Spin waves*, Springer, 2009.
- [8] Y Kajiwar, K Harii, S Takahashi, Jun-ichiro Ohe, K Uchida, M Mizuguchi, H Umezawa, H Kawai, Kazuya Ando, K Takanashi, et al., “Transmission of electrical signals by spin-wave interconversion in a magnetic insulator”, *Nature*, vol. 464, no. 7286, pp. 262–266, 2010.
- [9] Marcin Rytel, Paweł Kopyt, and Bartłomiej Salski, “Phase locked loop ku band frequency synthesizer based on a tuned yig oscillator”, in *2018 22nd International Mi-*

- crowave and Radar Conference (MIKON)*. IEEE, 2018, pp. 434–437.
- [10] CS Tsai, G Qiu, H Gao, LW Yang, GP Li, SA Nikitov, and Y Gulyaev, “Tunable wideband microwave band-stop and band-pass filters using yig/ggg-gaas layer structures”, *IEEE transactions on magnetics*, vol. 41, no. 10, pp. 3568–3570, 2005.
- [11] KL Kotzebue and LB Fletcher, “A ferrimagnetically-tuned parametric amplifier”, *IEEE Transactions on Microwave Theory and Techniques*, vol. 13, no. 6, pp. 773–776, 1965.
- [12] Sergio M Rezende and Flavio M de Aguiar, “Spin-wave instabilities, auto-oscillations, and chaos in yttrium-iron-garnet”, *Proceedings of the IEEE*, vol. 78, no. 6, pp. 893–908, 1990.
- [13] Sanchar Sharma, Yaroslav M Blanter, and Gerrit EW Bauer, “Optical cooling of magnons”, *Physical review letters*, vol. 121, no. 8, pp. 087205, 2018.
- [14] RL Jepsen, “Harmonic generation and frequency mixing in ferromagnetic insulators”, *Journal of Applied Physics*, vol. 32, no. 12, pp. 2627–2630, 1961.
- [15] Frederic R Morgenthaler, “Harmonic resonances in small ferrimagnetic ellipsoids”, *Journal of Applied Physics*, vol. 30, no. 4, pp. S157–S159, 1959.
- [16] Yi-Pu Wang, Guo-Qiang Zhang, Dengke Zhang, Tie-Fu Li, C-M Hu, and JQ You, “Bistability of cavity magnon polaritons”, *Physical review letters*, vol. 120, no. 5, pp. 057202, 2018.
- [17] Yi-Pu Wang, Guo-Qiang Zhang, Dengke Zhang, Xiao-Qing Luo, Wei Xiong, Shuai-Peng Wang, Tie-Fu Li, C-M Hu, and JQ You, “Magnon kerr effect in a strongly coupled cavity-magnon system”, *Physical Review B*, vol. 94, no. 22, pp. 224410, 2016.
- [18] P Hyde, BM Yao, YS Gui, Guo-Qiang Zhang, JQ You, and C-M Hu, “Direct measurement of foldover in cavity magnon-polariton systems”, *Physical Review B*, vol. 98, no. 17, pp. 174423, 2018.
- [19] H Suhl, “The theory of ferromagnetic resonance at high signal powers”, *Journal of Physics and Chemistry of Solids*, vol. 1, no. 4, pp. 209–227, 1957.
- [20] G Wiese and H Benner, “Multistability and chaos by parametric excitation of longwave modes in a yig sphere”, *Zeitschrift für Physik B Condensed Matter*, vol. 79, no. 1, pp. 119–131, 1990.
- [21] Mehrdad Elyasi, Yaroslav M Blanter, and Gerrit EW Bauer, “Resources of nonlinear cavity magnonics for quantum information”, *arXiv:1910.11130*, 2019.
- [22] Zhedong Zhang, Marlan O Scully, and Girish S Agarwal, “Quantum entanglement between two magnon modes via kerr nonlinearity driven far from equilibrium”, *Physical Review Research*, vol. 1, no. 2, pp. 023021, 2019.
- [23] Xufeng Zhang, Chang-Ling Zou, Liang Jiang, and Hong X Tang, “Strongly coupled magnons and cavity microwave photons”, *Physical review letters*, vol. 113, no. 15, pp. 156401, 2014.
- [24] Yutaka Tabuchi, Seiichiro Ishino, Toyofumi Ishikawa, Rekishu Yamazaki, Koji Usami, and Yasunobu Nakamura, “Hybridizing ferromagnetic magnons and microwave photons in the quantum limit”, *Physical Review Letters*, vol. 113, no. 8, pp. 083603, 2014.
- [25] Dany Lachance-Quirion, Yutaka Tabuchi, Arnaud Gloppe, Koji Usami, and Yasunobu Nakamura, “Hybrid quantum systems based on magnonics”, *Applied Physics Express*, vol. 12, no. 7, pp. 070101, 2019.
- [26] Dany Lachance-Quirion, Samuel Piotr Wolski, Yutaka Tabuchi, Shingo Kono, Koji Usami, and Yasunobu Nakamura, “Entanglement-based single-shot detection of a single magnon with a superconducting qubit”, *arXiv:1910.09096*, 2019.
- [27] Yutaka Tabuchi, Seiichiro Ishino, Atsushi Noguchi, Toyofumi Ishikawa, Rekishu Yamazaki, Koji Usami, and Yasunobu Nakamura, “Quantum magnonics: The magnon meets the superconducting qubit”, *Comptes Rendus Physique*, vol. 17, no. 7, pp. 729–739, 2016.
- [28] Silvia Viola Kusminskiy, “Cavity optomagnonics”, *arXiv:1911.11104*, 2019.
- [29] D. M. Berns, W. D. Oliver, S. O. Valenzuela, A. V. Shtyov, K. K. Berggren, L. S. Levitov, and T. P. Orlando, “Coherent quasiclassical dynamics of a persistent current qubit”, *Physical Review Letters*, vol. 97, no. 15, pp. 150502, 2006.
- [30] SN Shevchenko, S. Ashhab, and F. Nori, “Landau–zener–stückelberg interferometry”, *Physics Reports*, vol. 492, no. 1, pp. 1–30, 2010.
- [31] B Yurke, “Input-output theory”, in *Quantum Squeezing*, pp. 53–96. Springer, 2004.
- [32] Eyal Buks, Chunqing Deng, Jean-Luc F. X. Orgazzi, Martin Otto, and Adrian Lupascu, “Superharmonic resonances in a strongly coupled cavity-atom system”, *Phys. Rev. A*, vol. 94, pp. 033807, Sep 2016.
- [33] GuoQiang Zhang, YiPu Wang, and JianQiang You, “Theory of the magnon kerr effect in cavity magnonics”, *SCIENCE CHINA Physics, Mechanics & Astronomy*, vol. 62, no. 8, pp. 987511, 2019.
- [34] PC Fletcher and RO Bell, “Ferrimagnetic resonance modes in spheres”, *Journal of Applied Physics*, vol. 30, no. 5, pp. 687–698, 1959.
- [35] Bernard Yurke and Eyal Buks, “Performance of cavity-parametric amplifiers, employing kerr nonlinearities, in the presence of two-photon loss”, *J. Lightwave Tech.*, vol. 24, pp. 5054–5066, 2006.
- [36] Stephen Blundell, “Magnetism in condensed matter”, 2003.
- [37] T Holstein and HI Primakoff, “Field dependence of the intrinsic domain magnetization of a ferromagnet”, *Physical Review*, vol. 58, no. 12, pp. 1098, 1940.

